Available online at www.sciencedirect.com
ScienceDirect
Journal of Magnetic Resonance 187 (2007) 155–162
JMR Journal of Magnetic Resonance
www.elsevier.com/locate/jmr

Communication

Comparisons of EPR imaging and T_1-weighted MRI for efficient imaging of nitroxyl contrast agents

Ken-ichiro Matsumoto [a,*], Michiko Narazaki [b], Hiroo Ikehira [b], Kazunori Anzai [a], Nobuo Ikota [c]

[a] *Radiation Modifier Research Team, Heavy-Ion Radiobiology Research Group, Research Center for Charged Particle Therapy, National Institute of Radiological Sciences, 4-9-1 Anagawa, Inage-ku, Chiba-shi, Chiba 263-8555, Japan*
[b] *Magnetic Resonance Probing Section, Department of Biophysics, Molecular Imaging Center, National Institute of Radiological Sciences, 4-9-1 Anagawa, Inage-ku, Chiba-shi, Chiba 263-8555, Japan*
[c] *Director of Special Research, National Institute of Radiological Sciences, 4-9-1 Anagawa, Inage-ku, Chiba-shi, Chiba 263-8555, Japan*

Received 21 September 2006; revised 12 January 2007
Available online 24 March 2007

Abstract

The resolution and signal to noise ratio of EPR imaging and T_1-weighted MRI were compared using an identical phantom. Several solutions of nitroxyl contrast agents with different EPR spectral shapes were tested. The feasibility of T_1-weighted MRI to detect nitroxyl contrast agents was described. T_1-weighted MRI can detect nitroxyl contrast agents with a complicated EPR spectrum easier and quicker; however, T_1-weighted MRI has less quantitative ability especially for lipophilic nitroxyl contrast agents, because T_1-relaxivity, i.e. accessibility to water, is affected by the hydrophilic/hydrophobic micro-environment of a nitroxyl contrast agent. The less quantitative ability of T_1-weighted MRI may not be a disadvantage of redox imaging, which obtains reduction rate of a nitroxyl contrast. Therefore, T_1-weighted MRI has a great advantage to check the pharmacokinetics of newly modified and/or designed nitroxyl contrast agents.

Keywords: Nitroxyl radical; Redox-sensitive contrast agent; Magnetic resonance imaging; T_1-relaxivity; T_1-weighted contrast; Electron paramagnetic resonance imaging

1. Introduction

Nitroxyl free radical species are recommended as tissue redox-sensitive MR contrast agents [1]. Paramagnetic nitroxyl radicals have a proton T_1-shortening effect, which has been known since the early 1980s [2,3]. Nitroxyl free radicals are relatively stable radical species in an aqueous solution, while they are readily reduced to the corresponding diamagnetic hydroxylamine forms in biological systems; therefore, in vivo T_1-weighted MR contrasts were decreased depending on the reduction of nitroxyl radicals.

Nitroxyl radicals have been utilized as redox probes in the field of electron paramagnetic resonance (EPR) spectroscopy and imaging [4–11]. EPR can directly detect the absorbance of a microwave/radio frequency by electron spin on nitroxyl radical species. The in vivo time course of EPR signal intensity of a nitroxyl radical can be varied by reductive or oxidative environments in living tissues. Variation of the in vivo decay rate of EPR signal intensity of the nitroxyl radical reflects the modification of the in vivo redox status. Several nitroxyl radicals reported were blood–brain barrier permeable and can be functional contrast agents for the brain [12–15]. Although many reports have described the in vivo reduction and pharmacokinetics of nitroxyl radicals, the low anatomical resolution of EPR images could not ensure the tissue depending on the redox environments.

EPR spectral information must be removed with a conventional spatial EPR imaging technique to obtain pure spatial information. Theoretically, hyper-fine splitting

* Corresponding author. Fax: +81 43 255 6819.
E-mail address: matsumok@nirs.go.jp (K. Matsumoto).

1090-7807/$ - see front matter © 2007 Elsevier Inc. All rights reserved.
doi:10.1016/j.jmr.2007.03.013

(hfs) and the broad EPR linewidth of nitroxy radical can be removed using the deconvolution technique [16–18], while the low signal to noise ratio (S/N) of in vivo EPR imaging data is not suitable for the deconvolution process. In addition, the complicated hfs and broad linewidth make the S/N lower. Using the lower field gradient, EPR images can sometimes be obtained without the deconvolution process when one of the hfs peaks is chosen. In such cases, the EPR spectral linewidth directly contributes to the image, and lowers the image resolution. In addition, multiple spectral components coexisting in a sample make the conventional spatial EPR imaging invalid. Such cases have been seen with amphiphilic species (TEMPO, OXANO, MC-PROXYL, etc.), even though a single nitroxyl contrast agent was used in the experiment. The spectral-spatial EPR imaging technique can be employed to map multiple spectral distributions [19,20], while this technique requires more acquisition time. Spectral information and spatial information are alternatives in those EPR imaging techniques. To achieve higher S/N and higher image resolution for EPR imaging, a suitable paramagnetic contrast agent required a single-line EPR signal with quite a narrow linewidth; therefore, the application of EPR imaging has been limited to a complicated hfs, anisotropic spectrum, very broad linewidth, and/or mixture of such multiple conditions.

T_1-weighted MR contrasts can achieve a distribution mapping of a nitroxyl radical in tissue with detailed anatomical information [1]. There are no EPR spectral contributions in the mapping of nitroxyl contrast agent obtained by T_1-weighted MRI; therefore, technical limitations due to complications of the EPR spectral components are eliminated. For example, this is a marked advantage to design a new organ/tissue-specific redox-sensitive nitroxyl contrast agent. The other advantage of nitroxyl contrast agents is that their in vivo molecular modification can be easily checked with X-band or L-band EPR spectroscopic techniques. In this paper, several nitroxyl radical solutions with different EPR spectral characteristics were tested. EPR imaging and proton T_1-weighted MRI were compared. The feasibility of the MR detection of nitroxyl contrast agents was discussed.

2. Results and discussion

Fig. 1 shows a schematic drawing of a phantom. The phantom was assembled as a hexagonal lattice with 7 tubes containing a concentration series of a nitroxyl contrast agent. Fig. 2 shows L-band EPR spectra of the phantoms. Carbamoyl-PROXYL dissolved in PBS containing 1% BSA showed sharp triplet lines (Fig. 2a). Carboxy-PTIO dissolved in PBS containing 1% BSA showed 5 sharp lines with a ratio of 1:2:3:2:1 (Fig. 2b). Those nitroxyls can be dissolved in PBS and moved freely independent of BSA. On the other hand, the 5-DSA dissolved in PBS containing 1% BSA showed markedly low signal intensity with a broad linewidth due to strong anisotropy (Fig. 2c). This anisotropic spectrum did not show any recognizable triplet in the L-band EPR spectrum even at high magnification, although the X-band spectrum showed a trace (which was about 0.25% of the total) of triplet lines. The 5-DSA dissolved in PBS containing 1% SDS showed triplet lines with fewer anisotropic features (Fig. 2d).

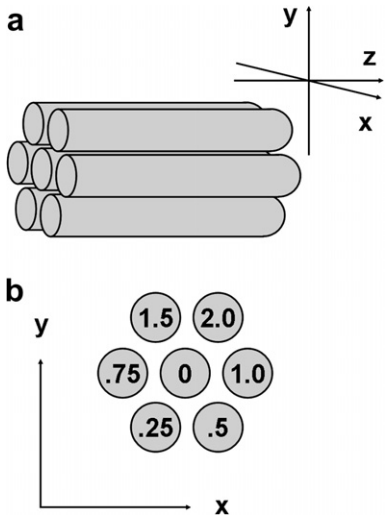

Fig. 1. A schematic drawing of a phantom assembled with seven tubes containing concentration series solutions of a nitroxyl contrast agent. (a) 3D display of the phantom. Seven tubes were assembled as a hexagonal lattice. (b) 2D display of x–y plane of the phantom. Numbers indicated in tubes are the concentrations of the contrast agent (mM). The center tube (indicated as 0 mM) contains buffer only. Six phantoms are prepared for six preparations of three nitroxyl contrast agents, i.e. carbamoyl-PROXYL, carboxy-PTIO, 5-DSA solved in PBS containing 1% BSA and those solved in PBS containing 1% SDS. All phantoms have identical geometry.

Fig. 3 shows EPR images of 3 phantoms obtained with a higher field gradient (1 mT/cm). Sufficient long sweep width (6.4 mT), which can cut a whole EPR spectrum shape, was employed. The EPR spectrum shape was deconvoluted from raw data to obtain spatial projection, which was used to reconstruct an image. An EPR image of the phantom consisting of carbamoyl-PROXYL showed relatively good image resolution and background noises, and/or artifacts were low (Fig. 3a). The EPR image of the phantom of carboxy-PTIO showed a slightly higher background, i.e. S/N became slightly lower, while image resolution could still acceptably distinguish each tube. The left panel of Fig. 3c shows an EPR image of the phantom of 5-DSA solution containing 1% BSA. Nothing can be distinguished in this image. The right panel of Fig. 3c was reconstructed from the same data of the left image, except that the deconvolution process was skipped. In the right image, traces of tubes can be seen but almost at the noise level. Fig. 3d is an EPR image of the phantom of 5-DSA solutions containing 1% SDS with the deconvolution process. Tubes can be seen in Fig. 3d, while background noise is very high. The background noise of Fig. 3c, left panel and d look similar. Deconvolution of a

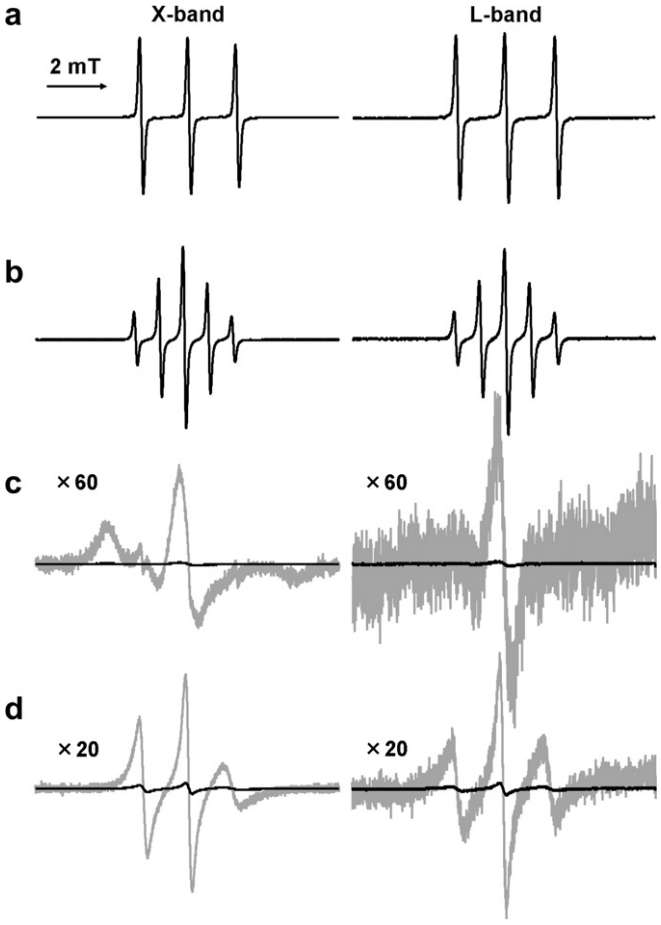

Fig. 2. L-band EPR spectra of the phantoms. Phantoms were assembled with a concentration series of 0–2 mM solutions of a nitroxide. (a) Carbamoyl-PROXYL in PBS containing 1% BSA showed sharp triplet lines. (b) Carboxy-PTIO in PBS containing 1% BSA showed five sharp lines. (c) 5-DSA in PBS containing 1% BSA showed an anisotropic spectrum typical of restricted motion, The peak height of which was markedly lower than that of the carbamoyl-PROXYL and the carboxy-PTIO. (d) 5-DSA in PBS containing 1% SDS showed anisotropic triplet lines. X-band EPR parameters were as follows: frequency = 9.4 GHz, center magnetic field = 336 mT, microwave power = 2.0 mW, field modulation frequency = 100 kHz, field modulation amplitude = 0.063 mT, time constant = 0.01 s, sweep width = 10 mT, scan time (sweep time) = 1 min. L-band EPR parameters were the same as X-band measurement except frequency = 1100 MHz, center magnetic field = 40 mT, and microwave power = 0.1 mW. An identical receiver gain was used for all measurements. Gray spectra indicated in (c) and (d) are magnifications of the corresponding spectra. Magnification rates are indicated in the figure.

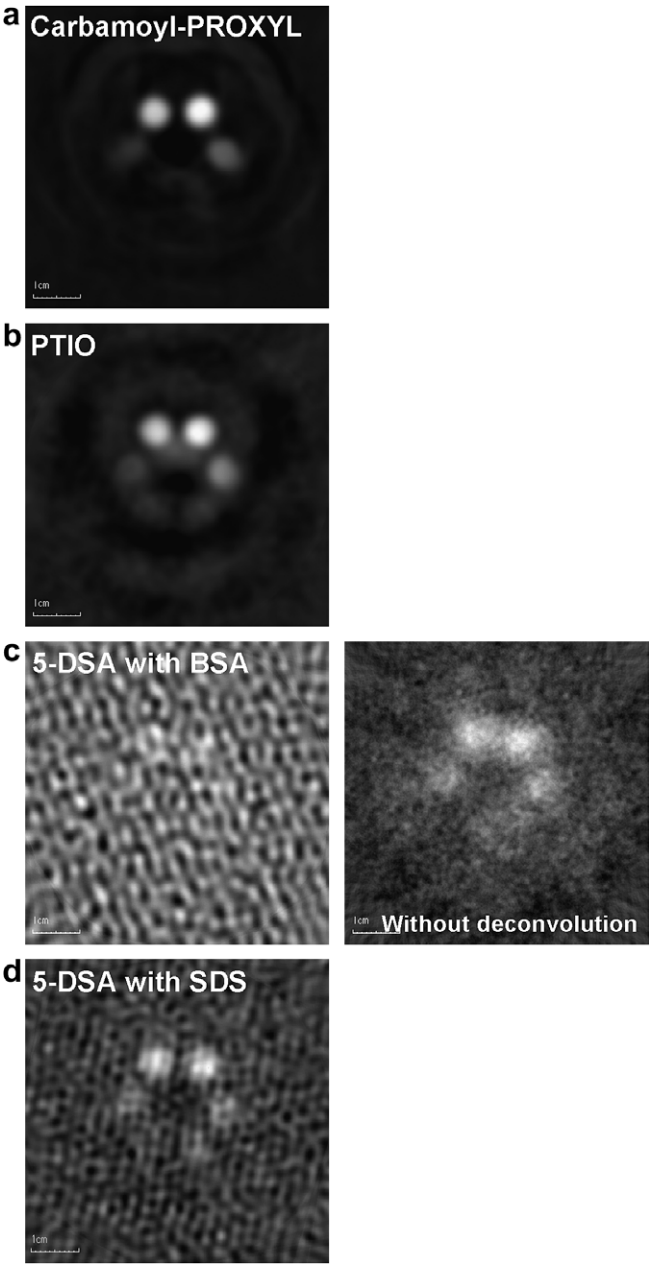

Fig. 3. EPR images obtained with field gradient and deconvolution process. A stable 1.0 mT/cm field gradient was rotated with a 2° angle step, then 90 projections were obtained. Images were reconstructed by filtered back-projection method with a Shepp-Logan filter. Field sweep width was 6.4 mT. Field of view was 6.4 × 6.4 cm. Dynamic ranges were 0 to the maximum value of each image. (a) Carbamoyl-PROXYL, (b) carboxy-PTIO, and (c) 5-DSA solved in PBS containing 1% BSA. (d) 5-DSA solved in PBS containing 1% SDS. The right panel of (c) was reconstructed using the same data as the left panel except that the deconvolution process was skipped. EPR parameters were as follows: microwave frequency was 1100 MHz, microwave power was 0.1 mW, modulation frequency was 100 kHz, modulation amplitude was 0.063 mT, time constant was <0.001 s, and sweep rate was 3.2 mT/s. Identical receiver gain was used for all measurements.

relatively broad linewidth, which is a low frequency component, retains high frequency noises.

Fig. 4 shows EPR images of the same 3 phantoms obtained with a lower field gradient (0.1875 mT/cm). The corresponding sweep width was 1.2 mT, which could cut only the center peak of the EPR spectrum; therefore, the deconvolution process was not employed and spectral data were directly used as image projections. Images of carbamoyl-PROXYL and carboxy-PTIO phantoms were blurred but some of the tubes can still be seen (Fig. 4a and b); however, no actual tube shape can be distinguished on the image of the 5-DSA phantom (Fig. 4c). Fig. 4d, which is the phantom of 5-DSA solutions containing 1% SDS, showed better convergence of distribution compared with Fig. 4c, while the resolution of the image was quite low.

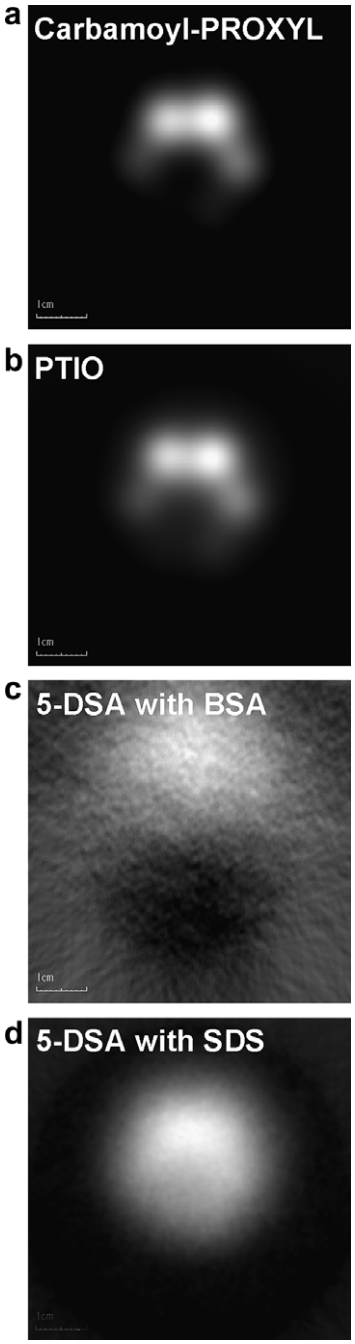

Fig. 4. EPR images obtained with a lower field gradient. The identical phantom used in Fig. 3 was sequentially scanned after the scan for Fig. 3 without any movement. Data were acquired under the following conditions. A stable 0.1875 mT/cm field gradient was rotated with a 2° angle step, then 90 projections were obtained. Images were reconstructed by the FBP method with a Shepp-Logan filter. Field sweep width was 1.2 mT. Field of view was 6.4×6.4 cm. Images were directly reconstructed using raw spectra as projections without a deconvolution process. Images were reconstructed by FBP with a Shepp-Logan filter. Dynamic ranges were 0 to the maximum value of each image. (a) Carbamoyl-PROXYL, (b) carboxy-PTIO, (c) 5-DSA solved in PBS containing 1% BSA. (d) 5-DSA solved in PBS containing 1% SDS. EPR parameters were the same as Fig. 2.

The left column of Fig. 5 shows R_1 mapping. The center column shows T_1-weighted images scanned by a FLASH sequence. The right column shows mapping of the signal enhancement level ($\Delta S\%$) defined as follows;

$$\Delta S\% = (\text{pixel signal intensity})/(\text{averaged signal intensity in center tube}) \times 100 - 100. \quad (1)$$

All images show quite high image resolution compared with corresponding EPR images.

When solutions of nitroxyl contrast agents were prepared by PBS buffer containing 1% BSA, all nitroxyl species showed a similar r_1 value (Fig. 6a) and signal enhancement levels (Fig. 6b) depending on the concentration of nitroxyl contrast agents, but not on the microenvironments of nitroxyl free radicals. When solutions of 5-DSA were prepared by PBS buffer containing 1% SDS, however, the r_1 value and signal enhancement levels were lower than those of the solution prepared by buffer containing 1% BSA.

The deconvolution process can eliminate spectral contribution and make the image resolution high, while simultaneously the process can simultaneously give relatively low frequency noise. Fig. 3a and b show an undulating background. The background undulation looks larger in Fig. 3b, i.e. PTIO. The left panel of Fig. 3c shows only ghosting, with the frequency appearing lower than the natural noise on the image of the right panel. Partly lower S/N in the 5 lines of PTIO and totally low S/N of broad 5-DSA spectrum may be a source of low frequency noise mediated by the deconvolution process. Hence, the complication of the hfs and a broadening of the linewidth may disturb the strict deconvolution process.

The combination of nitroxyl contrast agents and T_1-weighted MRI can improve not only the image quality (resolution and S/N) but also temporal resolution. A set of three slices was obtained by FLASH sequence which takes only 26 s in this experiment. Such rapid data acquisition has enabled pharmacokinetic imaging using TEMPOL [21]. In the case of TEMPOL, the rapid in vivo reduction rate and its broad EPR linewidth make in vivo EPR imaging of TEMPOL quite difficult.

The high anisotropic EPR spectrum of 5-DSA solved with BSA (Fig. 2c) suggests that 5-DSA molecules were adsorbed on the surface of BSA and a trace of free molecules can remain in the solution. Free 5-DSA in the solution was only 0.25% of the total, suggesting that the accessibility of 5-DSA molecules on the surface of BSA to water may be sufficiently fast, the same as free 5-DSA molecules; however, EPR spectra of 5-DSA solved with SDS (Fig. 2d) suggest that 5-DSA molecules were incorporated in SDS micelles. In this case, the percentage of MR signal enhancement and the T_1-relaxivity by 5-DSA were reduced, because the accessibility of 5-DSA to water molecules may be restricted; therefore, in vivo distribution of nitroxyl contrast agents to deep lipophilic sites may give weaker MR signal enhancement

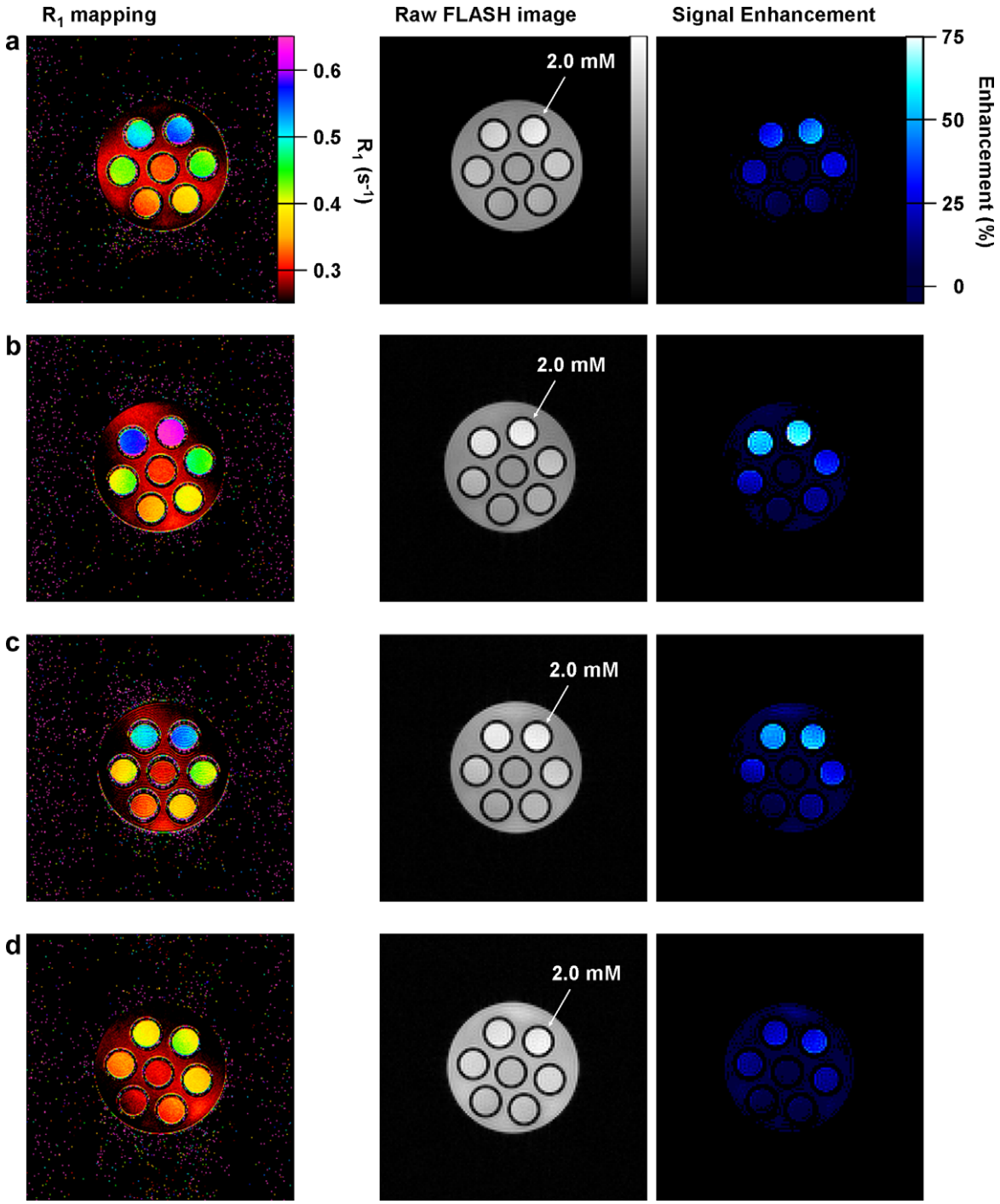

Fig. 5. R_1 mappings and T_1-weighted signal enhancement images. (a) Carbamoyl-PROXYL solved in PBS containing 1% BSA, (b) carboxy-PTIO solved in PBS containing 1% BSA, (c) 5-DSA solved in PBS containing 1% BSA, and (d) 5-DSA solved in PBS containing 1% SDS. The left column shows R_1 mappings. The middle column shows T_1-weighted images scanned by FLASH sequence. The right column shows mappings of signal enhancement level ($\Delta S\%$). $\Delta S\% =$ (pixel signal intensity)/(averaged signal intensity in center tube) $\times 100 - 100$. The phantoms were identical to those used in Figs. 3 and 4. The color bar indicated on the right side of (a) is common to all.

compared to hydrophilic sites. This suggests that in vivo quantification of nitroxyl contrast agents, especially lipophilic agents, using MRI, is difficult.

Carbamoyl-PROXYL and PTIO showed almost no (quite weak) anisotropy on X-band EPR spectra in either solution containing SDS or BSA (data not shown). The r_1 values of carbamoyl-PROXYL and carboxy-PTIO dissolved in PBS containing SDS (0.141 and 0.159 $mM^{-1}\ s^{-1}$, respectively) were similar to those dissolved in the PBS containing BSA (0.128 and 0.160 $mM^{-1}\ s^{-1}$, respectively);

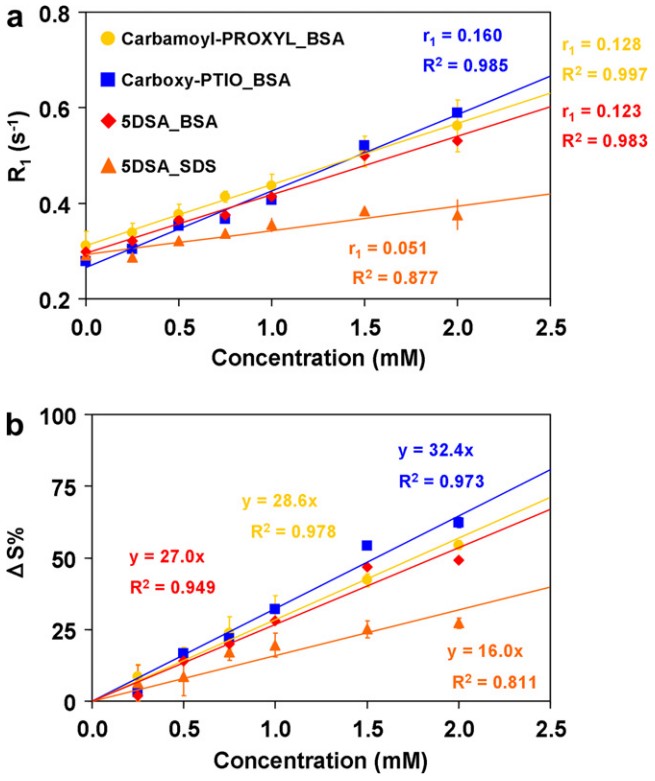

Fig. 6. The dependence of R_1 (a) and T_1-weighted signal enhancements (b) on the concentration of nitroxyl contrast agents. (a) Averaged signal intensity in each tube shown in left column of Fig. 5 and SD are indicated by markers and error bars. Circles, squares, and diamonds indicate carbamoyl-PROXYL, carboxy-PTIO, and 5-DSA solved in PBS containing 1% BSA, respectively. Triangles indicate 5-DSA solved in PBS containing 1% SDS. (b) Averaged signal intensity in each tube shown in right column of Fig. 5 and SD are indicated by markers and error bars. Indications of makes are common to (a).

therefore, these hydrophilic molecules mostly exist independently of SDS or BSA.

Adsorbing and/or dissolving nitroxyl contrast agents to large molecules and/or cell membranes can strongly be considered for in vivo situations, even though carbamoyl-PROXYL is employed. A previous paper [22] showed weak but recognizable anisotropy of carbamoyl-PROXYL in bile. Such a condition may make quantification of carbamoyl-PROXYL difficult and complicated, while MR redox imaging may not be affected by such anisotropy of the contrast agent. When the reduction rate of nitroxides was obtained from the slope of the semi-logarithmic plot of $\Delta S\%$ with time, the effect of the signal enhancement factor, i.e. relaxivity r_1, to the observed decay rate is sufficiently small to be negligible, theoretically; therefore, the different relaxivity of a nitroxyl contrast agent in different tissues can not be a disadvantage of in vivo MR redox imaging.

EPR spectral shapes do not have to be considered for a nitroxyl redox probe used in MR redox imaging. This can be a large advantage to modify nitroxyl contrast agents chemically and develop a tissue-specific redox probe. The detection of nitroxide by T_1-weighted MRI is quick and gives extremely good resolution compared with EPR imaging; however, the careful EPR spectroscopic analysis is required simultaneously to ensure information from MRI.

3. Conclusion

EPR imaging and T_1-weighted MRI to detect nitroxyl contrast agents were compared. The advantages and disadvantages of T_1-weighted MRI were revealed. S/N of the EPR image decreased depending on the complication of hfs and the linewidth (anisotropy). T_1-relaxivity levels of the nitroxyl contrast agents used in this study were similar in identical solvent. The T_1-weighted signal enhancement level ($\Delta S\%$) depended on nitroxyl spin concentration in the sample. The restriction of molecular movement by simple adhesion to a large molecule did not affect T_1-relaxivity so much, while solving a nitroxyl contrast agent into hydrophobic sites of micelles made T_1-relaxivity smaller.

T_1-weighted MRI can simplify the detection of nitroxyl contrast agents with a complicated EPR spectrum. This will be a great advantage to modify nitroxyl contrast agents chemically and to design organ/tissue specificity for in vivo use. Less quantification ability of T_1-weighted MRI may not be a severe problem for redox estimation; however, the support by EPR spectroscopy is necessary to understand MRI information correctly.

4. Materials and methods

4.1. Chemicals

Carbamoyl-PROXYL (3-carbamoyl-2,2,5,5-tetramethylpyrrolidine-*N*-oxyl) and 5-DSA (5-(*N*-oxyl-4′,4′-dimethyloxazolidine)-stearic acid) were purchased from Sigma–Aldrich Co. (St. Louis, MO, USA). Carboxy-PTIO (2-(4-carboxyphenyl)-4,4,5,5-tetramethylimidazoline-3-oxide-1-oxyl) was purchased from Dojindo Laboratories (Kumamoto, Japan). Other chemicals used were of analytical grade.

4.2. Phantom

Each contrast agent, carbamoyl-PROXYL, carboxy-PTIO, and 5-DSA, was dissolved in PBS containing 1% bovine serum albumin (BSA) or in PBS containing 1% sodium dodecyl sulfate (SDS) to prepare 2 mM standard solution. These 2 mM solutions were diluted with the corresponding buffer to obtain a series of concentrations (0, 0.25, 0.5, 0.75, 1.0, 1.5, and 2.0 mM). Each solution was put into a glass tube (i.d. = 6.4 mm, o.d. = 8.0 mm) and sealed air-tight without bubbles. Seven tubes containing a concentration series of a nitroxyl contrast agent were put together to make a hexagonal lattice (Fig. 1). Six phantoms were prepared for each preparation, i.e. carbamoyl-PROXYL with BSA, carboxy-PTIO with BSA, 5-DSA with BSA, carbamoyl-PROXYL with SDS, carboxy-PTIO with SDS, and 5-DSA with SDS.

4.3. X-band EPR measurement

The 1 mM solutions from each preparation were measured by X-band (9.4 GHz) EPR (JEOL, Akishima, Tokyo, Japan) with a TE-mode cavity. An aliquot (60 μL) of sample solution was transferred into capillary tube and positioned in the center of the TE-mode cavity using special sample holder. Measurements were made under the following conditions: microwave frequency = 9.4 GHz, magnetic field strength = 336 mT, microwave power = 2.0 mW, field modulation frequency = 100 kHz, field modulation amplitude = 0.063 mT, time constant = 0.01 s, sweep width = 10 mT, scan time (sweep time) = 1 min.

4.4. L-band EPR measurement and imaging

L-band EPR measurements and imaging were performed at 1.2 GHz CW EPR (JEOL, Akishima, Tokyo, Japan) with a loop-gap resonator (i.d. 43 mm, length 28 mm). The phantom was positioned in the center of the loop-gap resonator, and measured under the following conditions: microwave frequency = 1100 MHz, magnetic field strength = 40 mT, microwave power = 0.1 mW, field modulation frequency = 100 kHz, field modulation amplitude = 0.063 mT, time constant = 0.01 s, sweep width = 10 mT, scan time (sweep time) = 1 min. For EPR imaging, a set of 90 projections rotated over 180° with a 2° angle step was obtained. The magnitude of the field gradient was 1.0 or 0.1875 mT/cm, and the sweep width was 6.4 or 1.2 mT, respectively. The scan time (sweep time) was 2 s/projection. The total scan time for an EPR image was 270 s. EPR images were reconstructed on a 512×512 matrix by filtered back-projection (FBP) using a Shepp-Logan filter. The FOV was 6.4×6.4 cm.

4.5. Proton T_1 mapping and T_1-weighted FLASH imaging

MRI measurements performed at 7.0 T were controlled with ParaVision® 3.0.2 (Bruker BioSpin MRI GmbH, Rheinstetten, Germany). The scanner was equipped with a BS20 shim coil (Bruker) and BGA12 gradient coil (Bruker). The maximum gradient of the system was 40 G/cm. To obtain R_1 values of samples, spin-echo images were obtained using a multi-slice multi-echo (MSME) sequence with TR = 6400, 3200, 1600, 800, 400 and 200 ms with TE = 15 ms. Image resolution of the phase-encoding dimension was 256 and the gradient encoding dimension was 192, FOV was 6.4×6.4 cm, image was reconstructed to 256×256 matrix, pixel resolution was $0.25\ \text{mm} \times 0.25$ mm, slice thickness was 2.0 mm. The fast low angle shot (FLASH) (TR = 50 ms, TE = 3.1 ms, FA = 50°, $N_{EX} = 4$) was employed for the acquisition of T_1-weighted images. Image resolution of the phase-encoding dimension was 128 and the gradient-encoding dimension was 128, FOV was 6.4×6.4 cm, pixel resolution was 128×128, and slice thickness was 2 mm. The scan time of FLASH was 26 s.

4.6. Image handling

EPRI and MRI data were analyzed using the ImageJ software package (a public domain Java image processing program inspired by NIH Image that can be extended by plug-ins, http://rsb.info.nih.gov/ij/).

References

[1] K. Matsumoto, F. Hyodo, A. Matsumoto, A.P. Koretsky, A.L. Sowers, J.B. Mitchell, M.C. Krishna, High-resolution mapping of tumor redox status by magnetic resonance imaging using nitroxides as redox-sensitive contrast agents, Clin. Cancer Res. 12 (2006) 2455–2462.

[2] R.C. Brasch, D.E. Nitecki, M. Brant-Zawadzki, D.R. Enzmann, G.E. Wesbey, T.N. Tozer, L.D. Tuck, C.E. Cann, J.R. Fike, P. Sheldon, Brain nuclear magnetic resonance imaging enhanced by a paramagnetic nitroxide contrast agent: preliminary report, AJR 141 (1983) 1019–1023.

[3] R.C. Brasch, D.A. London, G.E. Wesbey, T.N. Tozer, D.E. Nitecki, R.D. Williams, J. Doemeny, L.D. Tuck, D.P. Lallemand, Work in progress: nuclear magnetic resonance study of paramagnetic nitroxide contrast agent for enhancement of renal structures in experimental animals, Radiology 147 (1983) 773–779.

[4] K. Yasukawa, K. Kasazaki, F. Hyodo, H. Utsumi, Non-invasive analysis of reactive oxygen species generated in rats with water immersion restraint-induced gastric lesions using in vivo electron spin resonance spectroscopy, Free Radic. Res. 38 (2004) 147–155.

[5] T. Mikuni, G. He, S. Petryakov, M.M. Fallouh, Y. Deng, R. Ishihara, P. Kuppusamy, M. Tatsuta, J.L. Zweier, In vivo detection of gastric cancer in rats by electron paramagnetic resonance imaging, Cancer Res. 64 (2004) 6495–6502.

[6] M. Elas, A. Parasca, D.J. Grdina, H.J. Halpern, Oral administration is as effective as intraperitoneal administration of amifostine in decreasing nitroxide EPR signal decay in vivo, Biochim. Biophys. Acta 1637 (2003) 151–155.

[7] K. Yamada, P. Kuppusamy, S. English, J. Yoo, A. Irie, S. Subramanian, J.B. Mitchell, M.C. Krishna, Feasibility and assessment of non-invasive in vivo redox status using electron paramagnetic resonance imaging, Acta Radiol. 43 (2002) 433–440.

[8] G. Ilangovan, H. Li, J.L. Zweier, P. Kuppusamy, In vivo measurement of tumor redox environment using EPR spectroscopy, Mol. Cell. Biochem. 234–235 (2002) 393–398.

[9] P. Kuppusamy, H. Li, G. Ilangovan, A.J. Cardounel, J.L. Zweier, K. Yamada, M.C. Krishna, JB. Mitchell, Noninvasive imaging of tumor redox status and its modification by tissue glutathione levels, Cancer Res. 62 (2002) 307–312.

[10] S. Kazama, G. Takashige, H. Yoshioka, H. Tanizawa, T. Ogata, J. Koscielniak, LJ. Berliner, Dynamic electron spin resonance (ESR) imaging of the distribution of spin labeled dextran in a mouse, Magn. Reson. Med. 36 (1996) 547–550.

[11] H.J. Halpern, D.R. Jaffe, T.D. Nguyen, D.J. Haraf, D.P. Spencer, M.K. Bowman, R.R. Weichselbaum, AM. Diamond, Measurement of bioreduction rates of cells with distinct responses to ionizing radiation and cisplatin, Biochim. Biophys. Acta 1093 (1991) 121–124.

[12] K. Anzai, K. Saito, K. Takeshita, S. Takahashi, H. Miyazaki, H. Shoji, M.C. Lee, T. Masumizu, T. Ozawa, Assessment of ESR-CT imaging by comparison with autoradiography for the distribution of a blood–brain-barrier permeable spin probe, MC-PROXYL, to rodent brain, Magn. Reson. Imaging 21 (2003) 765–772.

[13] H. Sano, M. Naruse, K. Matsumoto, T. Oi, H. Utsumi, A new nitroxyl-probe with high retention in the brain and its application for brain imaging, Free Radic. Biol. Med. 28 (2000) 959–969.

[14] H. Yokoyama, O. Itoh, T. Ogata, H. Obara, H. Ohya-Nishiguchi, H. Kamada, Temporal brain imaging by a rapid scan ESR-CT system in rats receiving intraperitoneal injection of a methyl ester nitroxide radical, Magn. Reson. Imaging 15 (1997) 1079–1084.
[15] M. Hiramatsu, K. Oikawa, H. Noda, A. Mori, T. Ogata, H. Kamada, Free radical imaging by electron spin resonance computed tomography in rat brain, Brain Res. 697 (1995) 44–47.
[16] M.J.R. Hoch, Electron spin resonance imaging of paramagnetic centres in solids, J. Phys. C Solid State Phys. 14 (1981) 5659–5666.
[17] K. Ohno, A method of EPR imaging: application to spatial distributions of hydrogen atoms trapped in sulfuric acid ices, Jpn. J. Appl. Phys. 20 (1981) L179–L182.
[18] K. Ohno, ESR imaging: a deconvolution method for hyperfine patterns, J. Magn. Reson. 50 (1982) 145–150.
[19] K. Matsumoto, T. Yahiro, K. Yamada, H. Utsumi, In vivo EPR spectroscopic imaging for a liposomal drug delivery system, Magn. Reson. Med. 53 (2005) 1158–1165.
[20] K. Matsumoto, H. Utsumi, Development of separable electron spin resonance-computed tomography imaging for multiple radical species: an application to ·OH and ·NO, Biophys. J. 79 (2000) 3341–3349.
[21] F. Hyodo, K. Matsumoto, A. Matsumoto, J.B. Mitchell, M.C. Krishna, Probing the intracellular redox status of tumors with magnetic resonance imaging and redox-sensitive contrast agents, Cancer Res. 66 (2006) 9921–9928.
[22] K. Matsumoto, A. Okajo, T. Kobayahi, J.B. Mitchell, M.C. Krishna, K. Endo, Estimation of free radical formation by β-ray irradiation in rat liver, J. Biochem. Biophys. Method 63 (2005) 79–90.